Synthesis and Structural Characterisation of $[Pt_2Au_2(PPh_3)_4(CNC_6H_3Me_2\text{-}2,6)_4][PF_6]_2$; a Platinum–Gold Cluster with a Distorted Butterfly Geometry†

Clive E. Briant, David I. Gilmour, and D. M. P. Mingos*
Inorganic Chemistry laboratory, University of Oxford, South Parks Road, Oxford OX1 3QR

The complex $[Pt_2Au_2(PPh_3)_4(CNC_6H_3Me_2\text{-}2,6)_4][PF_6]_2$ has been synthesised from $[Pt(PPh_3)_2(C_2H_4)]$ and $[Au(CNC_6H_3Me_2\text{-}2,6)_2]^+$ in acetone. The cluster crystallises in the triclinic space group $P\bar{1}$ with two formula units and the unit cell of dimensions a = 13.882(4), b = 15.460(2), c = 27.578(5) Å, α = 77.99(5), β = 88.95(2), and γ = 67.41(5)°. The metal atoms define a distorted flattened butterfly with the gold atoms occupying the higher connectivity sites and forming a short gold–gold bond of length 2.593(2) Å. The platinum–gold distances lie in the range 2.712(2)—3.028(2) Å reflecting a distortion of the skeletal geometry from D_{2h} to C_{2v}. ^{31}P-{^1H} and ^{195}Pt-{^1H} n.m.r. studies suggest that in solution a symmetric D_{2h} structure is adopted in which the gold atoms are equivalent.

Although a large number of heteronuclear clusters of gold with Group 8 metals have been synthesised [1] no examples of cluster compounds of gold with palladium or platinum had been structurally characterised when the current research project was initiated.[2] Nyholm and co-workers [3] reported that $[Pt(PPh_3)_3]$ undergoes an oxidative-addition reaction with $[Au(PPh_3)Cl]$ to give $[Pt\{Au(PPh_3)\}Cl(PPh_3)_2]$,[4] however little spectroscopic evidence was presented to support the structure. This paper reports the investigation of the related oxidative-addition reactions of $[Pt(PPh_3)_2(C_2H_4)]$ with $[Au(CNC_6H_3Me_2\text{-}2,6)_2]X$ (X = PF_6^- or BF_4^-). A preliminary report of these results has been published.[5]

Since this work was initiated other gold–platinum clusters have been reported by Braunstein *et al.*[5] and Mingos and Wardle.[6,7] Braunstein *et al.*[5] reported the synthesis and structural characterisation of $[PtAu_2Cl(PEt_3)_2(PPh_3)_2]^+$ (**1**),

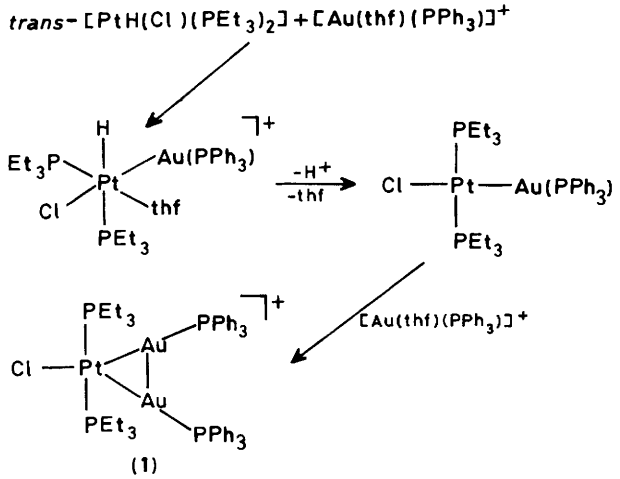

(1)

and proposed the sequence of reactions shown below to account for its formation (thf = tetrahydrofuran). Mingos and Wardle[6,7] reported the formation of 54- and 56-electron

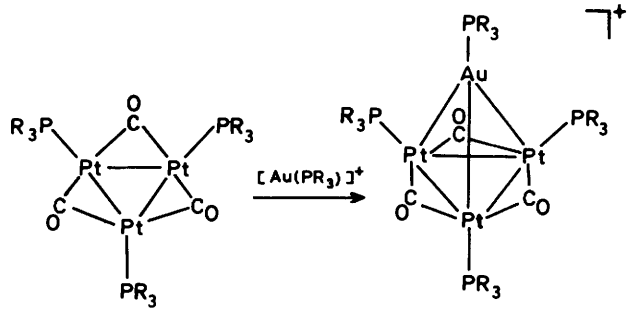

(2)

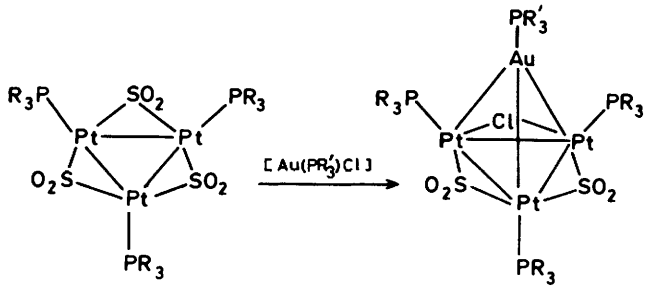

(3)

tetranuclear clusters of gold and platinum [(**2**) and (**3**)] by the routes shown above (R = C_6H_{11}, R′ = C_6H_4F-*p*). The compounds were characterised by single-crystal *X*-ray crystallographic studies and n.m.r. measurements.

Results and Discussion

The reaction of $[Au(CNC_6H_3Me_2\text{-}2,6)_2]X$ (X = BF_4^- or PF_6^-) with $[Pt(PPh_3)_2(C_2H_4)]$ in acetone in a 1:1 molar ratio gave a deep red solution. After stirring for 1 h, addition of diethyl ether precipitated dark brown crystals of $[Pt_2Au_2(PPh_3)_4(CNC_6H_3Me_2\text{-}2,6)_4]X_2$ [X = BF_4^- (**4a**) or PF_6^- (**4b**)] in 60% yield. The PF_6^- salt was also synthesised by metathesis of the BF_4^- salt with NH_4PF_6 in ethanol. The yield of (**4**) was reduced dramatically when free isocyanide was added, and yellow crystals of $[Pt_3(PPh_3)_2(CNC_6H_3Me_2\text{-}2,6)_6]X_2$ [X = BF_4^- (**5a**) or PF_6^- (**5b**)] were isolated in low yield under these conditions. Compound (**5b**) has been characterised by

† Di-μ-[bis(2,6-dimethylphenyl isocyanide)(triphenylphosphine)-platinio]-bis(triphenylphosphinegold) bis(hexafluorophosphate) (*Au-Au*).

Supplementary data available (No. SUP 56443, 10 pp.): thermal parameters, full list of bond lengths and angles. See Instructions for Authors, *J. Chem. Soc., Dalton Trans.*, 1986, Issue 1, pp. xvii—xx. Structure factors are available from the editorial office.

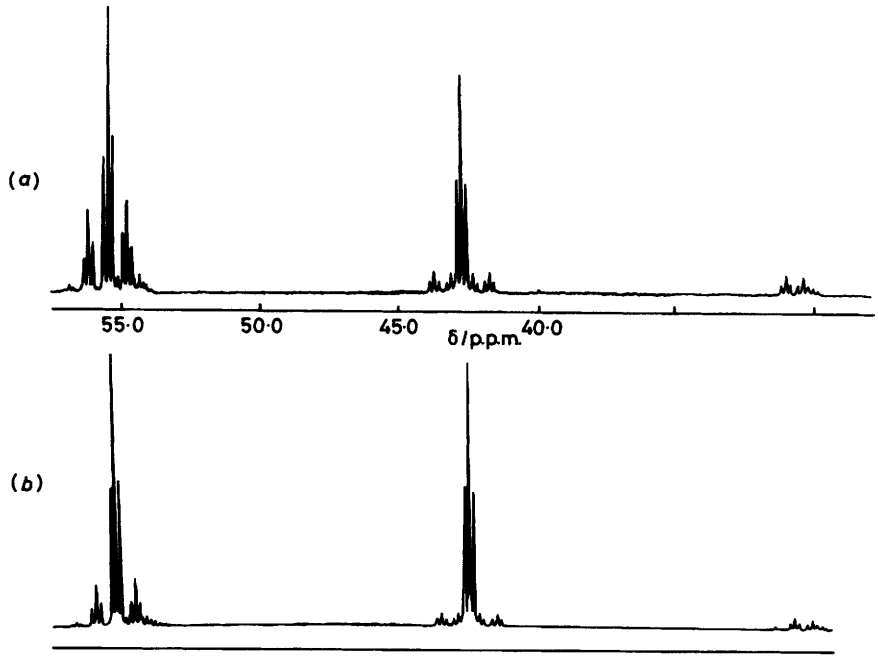

Figure 1. (*a*) Observed and (*b*) calculated $^{31}P-\{^1H\}$ spectra for $[Pt_2Au_2(PPh_3)_4(CNC_6H_3Me_2\text{-}2,6)_4][PF_6]_2$ (**4b**)

analytical data and single-crystal *X*-ray crystallographic measurements.[8]

The i.r. spectra (Nujol mull) of (**4a**) and (**4b**) showed the presence of terminal isocyanides [ν(CN) 2 130 cm^{-1}]. The *X*-ray fluorescence spectrum consisted of two peaks in a 1:1 ratio at the Au and Pt L_α lines. The $^{31}P-\{^1H\}$ n.m.r. spectrum of (**4b**) shows two resonances centred at 55.4 and 42.8 p.p.m. (relative to trimethyl phosphate) in a 1:1 ratio [see Figure 1(*a*)]. The resonance centred at 42.8 p.p.m. shows satellites which can be associated with ^1J(P–Pt) couplings and is therefore assigned to the phosphorus atom attached to platinum. The low-field satellite lies close to the resonance of the phosphorus attached to gold at 55.4 p.p.m. The spectrum has been satisfactory simulated using a computer analysis based on the spin systems A_2B_2 (isotopomer with no ^{195}Pt nucleus), $AA'B_2X$ (isotopomer with one ^{195}Pt nucleus X), and $AA'B_2XX'$ (isotopomer with two ^{195}Pt nuclei) [see Figure 1(*b*)]. The $^{195}Pt-\{^1H\}$ n.m.r. spectrum shows a broad doublet of doublets centred at −3 782.2 p.p.m. (relative to $Na_2[PtCl_6]$). The coupling constants derived from the computer analysis are given in Table 1. The magnitude of $^4J(P_{Pt}\text{–}P_{Pt})$ (61.0 Hz) compared with $^3J(P_{Pt}\text{–}P_{Au})$ (16.0 Hz) suggests the D_{2h} structure shown below (R = $C_6H_3Me_2$-2,6) in solution with the platinum phosphines *trans*.

The single-crystal *X*-ray crystallographic study of (**4b**) has confirmed the gross features of the structure although a detailed inspection of the bond lengths shows significant distortions of the type indicated by (**I**) (R = $C_6H_3Me_2$-2,3).

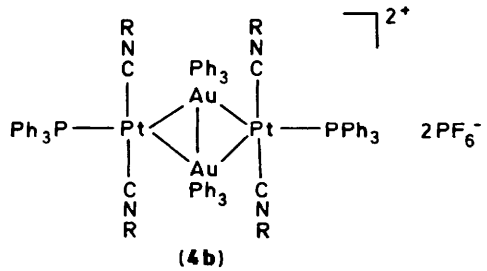

(**4b**)

Table 1. Chemical shifts and coupling constants for $[Pt_2Au_2(PPh_3)_4(CNC_6H_3Me_2\text{-}2,6)_4][PF_6]_2$ (**4b**)

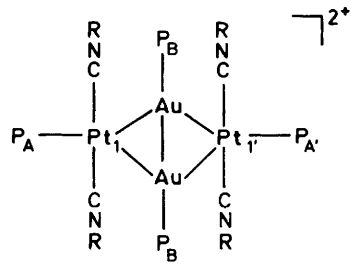

	$P_A/P_{A'}$	P_B	$Pt_1/Pt_{1'}$
δ/p.p.m.	42.8(m)	55.4(m)	−3 782.2 (d of d)

J/Hz		Pt_1	Pt_1	P_B	P_A
	P_A	2 384.0	137.0	16.0	61.0
	P_A	137.0	2 384.0	16.0	
	P_B	142.0	142.0		
	Pt_1	*			

* $^2J(Pt_1\text{–}Pt_1)$ could not be estimated from either the $^{31}P-\{^1H\}$ or $^{195}Pt-\{^1H\}$ spectra.

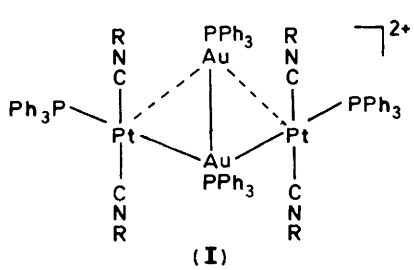

(**I**)

Table 2. Final fractional co-ordinates ($\times 10^4$) for non-hydrogen atoms of $[Pt_2Au_2(PPh_3)_4(CNC_6H_3Me_2\text{-}2,6)_4][PF_6]_2$ (**4b**) with estimated standard deviations in parentheses

Atom	*X/a*	*Y/b*	*Z/c*	Atom	*X/a*	*Y/b*	*Z/c*
Pt(1)	230(1)	1 948.3(9)	3 169.7(5)	C(115)	−1 559(27)	−1(20)	2 138(12)
Pt(2)	1 969(1)	−544.1(9)	2 177.6(5)	C(120)	−1 666(19)	366(18)	3 388(10)
Au(1)	531(1)	420.9(9)	2 757.2(5)	C(121)	−2 700(24)	561(25)	3 244(12)
Au(2)	1 667(1)	1 337.7(9)	2 356.6(5)	C(122)	−3 507(20)	1 118(27)	3 505(13)
P(1)	−571(7)	−336(6)	3 064(3)	C(123)	−3 264(23)	1 507(26)	3 877(13)
P(2)	−127(7)	2 959(6)	3 725(3)	C(124)	−2 230(25)	1 295(24)	4 013(11)
P(3)	2 468(7)	2 243(6)	1 903(3)	C(125)	−1 437(19)	772(22)	3 753(11)
P(4)	2 911(6)	−1 710(6)	1 752(3)	C(130)	36(21)	−1 468(17)	3 500(10)
P(5)	−6 356(9)	4 151(8)	4 250(4)	C(131)	989(23)	−2 104(21)	3 384(11)
P(6)	7 716(9)	−2 461(8)	762(4)	C(132)	1 467(21)	−3 025(20)	3 676(12)
F(1)	−6 210(20)	3 136(15)	4 194(9)	C(133)	990(25)	−3 305(19)	4 087(12)
F(2)	−5 382(19)	3 731(19)	4 619(9)	C(134)	42(24)	−2 672(21)	4 211(10)
F(3)	−5 693(20)	4 268(20)	3 806(9)	C(135)	−448(19)	−1 764(19)	3 904(11)
F(4)	−6 498(21)	5 154(16)	4 313(10)	C(210)	−1 378(19)	3 358(20)	3 993(10)
F(5)	−7 338(17)	4 574(18)	3 893(8)	C(211)	−1 479(23)	3 537(26)	4 463(12)
F(6)	−7 030(23)	4 047(22)	4 689(10)	C(212)	−2 467(27)	3 907(28)	4 644(11)
F(7)	6 772(26)	−2 476(27)	1 039(14)	C(213)	−3 351(21)	4 165(25)	4 338(13)
F(8)	7 119(17)	−2 139(16)	248(8)	C(214)	−3 256(23)	3 973(27)	3 867(12)
F(9)	8 670(26)	−2 404(29)	499(14)	C(215)	−2 255(28)	3 552(27)	3 691(11)
F(10)	8 088(24)	−3 518(18)	741(12)	C(220)	−15(27)	4 102(20)	3 462(12)
F(11)	8 348(20)	−2 794(20)	1 273(9)	C(221)	618(25)	4 102(20)	3 063(12)
F(12)	7 375(25)	−1 406(18)	777(13)	C(222)	753(29)	4 943(26)	2 835(13)
N(1)	177(21)	444(18)	1 363(10)	C(223)	190(32)	5 793(22)	2 976(14)
N(2)	2 178(22)	430(20)	3 810(10)	C(224)	−459(32)	5 795(23)	3 368(16)
N(3)	−1 707(23)	3 164(20)	2 469(11)	C(225)	−588(29)	4 948(27)	3 603(13)
N(4)	3 717(23)	−1 301(19)	3 019(11)	C(230)	777(21)	2 408(19)	4 284(10)
C(1)	776(27)	74(24)	1 715(13)	C(231)	743(21)	1 564(20)	4 578(11)
C(2)	1 480(23)	968(21)	3 546(11)	C(232)	1 458(24)	1 054(19)	4 984(11)
C(3)	−922(27)	2 696(24)	2 725(13)	C(233)	2 189(24)	1 388(23)	5 102(11)
C(4)	3 033(24)	−968(21)	2 715(11)	C(234)	2 207(24)	2 243(23)	4 826(12)
C(11)	−679(30)	962(27)	1 023(14)	C(235)	1 511(24)	2 751(19)	4 404(11)
C(12)	−1 210(29)	1 929(27)	1 020(14)	C(310)	1 571(22)	3 066(20)	1 388(10)
C(13)	−2 077(37)	2 448(33)	670(18)	C(311)	736(27)	3 881(25)	1 469(11)
C(14)	−2 356(36)	1 968(35)	357(17)	C(312)	22(26)	4 494(22)	1 075(14)
C(15)	−1 802(37)	1 068(34)	348(17)	C(313)	70(28)	4 241(26)	621(12)
C(16)	−920(28)	493(26)	684(17)	C(314)	890(34)	3 432(31)	540(12)
C(17)	−882(30)	2 385(27)	1 368(13)	C(315)	1 646(25)	2 846(23)	923(13)
C(18)	−307(33)	−510(31)	691(16)	C(320)	2 842(24)	2 987(20)	2 215(11)
C(21)	2 973(24)	−254(21)	4 187(11)	C(321)	2 886(25)	3 858(21)	1 955(9)
C(22)	2 774(24)	−995(22)	4 465(12)	C(322)	3 278(29)	4 373(20)	2 206(11)
C(23)	3 594(28)	−1 681(24)	4 825(13)	C(323)	3 611(27)	4 017(22)	2 706(11)
C(24)	4 475(29)	−1 482(26)	4 869(14)	C(324)	3 539(32)	3 163(25)	2 961(10)
C(25)	4 619(29)	−707(28)	4 597(14)	C(325)	3 143(27)	2 661(20)	2 712(12)
C(26)	3 835(29)	−23(26)	4 239(13)	C(330)	3 655(19)	1 604(18)	1 620(10)
C(27)	1 782(29)	−1 144(26)	4 389(14)	C(331)	4 342(30)	2 042(21)	1 444(16)
C(28)	3 950(32)	862(30)	3 935(16)	C(332)	5 214(26)	1 563(24)	1 189(14)
C(31)	−2 631(25)	3 834(23)	2 126(12)	C(333)	5 393(23)	659(23)	1 123(12)
C(32)	−3 330(30)	3 446(28)	1 989(14)	C(334)	4 737(25)	218(18)	1 316(13)
C(33)	−4 147(34)	4 153(34)	1 676(16)	C(335)	3 863(21)	696(19)	1 559(11)
C(34)	−4 157(34)	5 001(33)	1 488(16)	C(410)	2 204(22)	−2 409(21)	1 597(11)
C(35)	−3 469(34)	5 369(30)	1 605(16)	C(411)	1 288(25)	−2 351(23)	1 832(12)
C(36)	−2 587(26)	4 737(24)	1 940(13)	C(412)	705(23)	−2 860(25)	1 727(12)
C(37)	−3 305(41)	2 565(40)	2 245(21)	C(413)	998(27)	−3 377(25)	1 362(14)
C(38)	−1 811(33)	5 075(29)	2 102(15)	C(414)	1 871(29)	−3 384(27)	1 100(13)
C(41)	4 635(24)	−1 670(21)	3 317(11)	C(415)	2 466(22)	−2 881(24)	1 213(12)
C(42)	4 856(25)	−2 487(23)	3 695(12)	C(420)	3 339(21)	−1 257(19)	1 147(9)
C(43)	5 821(31)	−2 844(26)	3 978(14)	C(421)	4 233(22)	−1 802(18)	947(11)
C(44)	6 497(29)	−2 437(28)	3 886(14)	C(422)	4 504(23)	−1 431(22)	482(12)
C(45)	6 287(34)	−1 631(32)	3 515(17)	C(423)	3 915(27)	−513(23)	233(11)
C(46)	5 345(26)	−1 227(23)	3 223(12)	C(424)	3 007(26)	35(20)	421(12)
C(47)	4 108(27)	−2 953(24)	3 801(13)	C(425)	2 732(21)	−323(20)	890(11)
C(48)	5 143(30)	−376(28)	2 801(15)	C(430)	4 118(18)	−2 611(17)	2 083(9)
C(110)	−1 208(24)	−642(21)	2 596(10)	C(431)	4 977(23)	−2 377(19)	2 126(11)
C(111)	−1 373(22)	−1 496(18)	2 699(9)	C(432)	5 795(22)	−2 972(22)	2 483(12)
C(112)	−1 929(27)	−1 680(20)	2 337(12)	C(433)	5 806(22)	−3 844(21)	2 754(12)
C(113)	−2 271(28)	−1 042(24)	1 883(11)	C(434)	4 940(23)	−4 098(19)	2 721(11)
C(114)	−2 116(26)	−198(21)	1 783(10)	C(435)	4 098(19)	−3 463(19)	2 381(11)

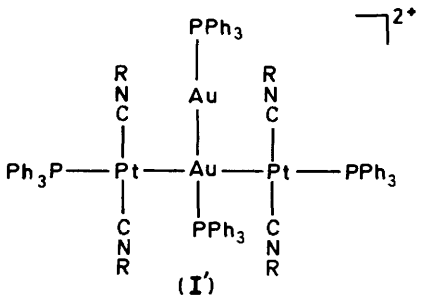

(I')

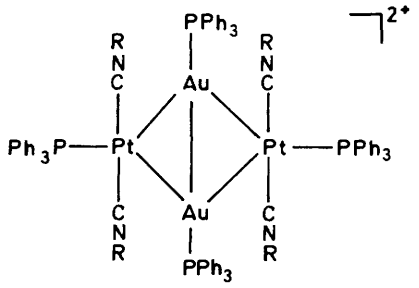

(II)

Table 3. Selected molecular dimensions (Å) and bond angles (°) for $[Pt_2Au_2(PPh_3)_4(CNC_6H_3Me_2\text{-}2,6)_4][PF_6]_2$ (**4b**) with estimated standard deviations in parentheses

Au(1)–Au(2)	2.593(2)	Au(1)–P(1)	2.310(8)
Pt(1)–Au(1)	2.718(2)	Au(2)–P(3)	2.276(9)
Pt(1)–Au(2)	3.028(2)	Pt(1)–C(2)	1.94(3)
Pt(2)–Au(1)	2.712(2)	Pt(1)–C(3)	1.86(4)
Pt(2)–Au(2)	2.922(2)	Pt(2)–C(1)	1.91(4)
Pt(1)–P(2)	2.324(8)	Pt(2)–C(4)	1.93(3)
Pt(2)–P(4)	2.313(8)		
Pt(1)–Au(1)–Pt(2)	134.97(6)	P(2)–Pt(1)–C(3)	97(1)
Pt(1)–Au(1)–Au(2)	69.49(5)	C(2)–Pt(1)–C(3)	167(1)
Au(1)–Pt(1)–Au(2)	53.31(4)	C(4)–Pt(2)–P(4)	94.7(9)
Au(1)–Pt(2)–Au(2)	54.65(4)	C(1)–Pt(2)–C(4)	169(1)
Pt(1)–Au(2)–Pt(2)	114.90(5)	P(1)–Au(1)–Au(2)	175.7(2)
Pt(1)–Au(2)–Au(1)	57.21(5)	Au(1)–Au(2)–P(2)	170.9(2)
Pt(2)–Au(2)–Au(1)	58.55(5)	P(2)–Pt(1)–Au(1)	162.9(2)
Au(2)–Au(1)–Pt(2)	66.80(5)	P(4)–Pt(2)–Au(1)	160.9(2)
P(2)–Pt(1)–C(2)	95.2(9)	P(1)–Au(1)–Pt(2)	113.3(2)
		P(1)–Au(1)–Pt(1)	111.1(2)

$$[Au(CNR)_2]^+ + [Pt(PPh_3)_2(C_2H_4)] \longrightarrow [Au(PPh_3)(CNR)]^+ + [Pt(PPh_3)(CNR)] + C_2H_4$$

$$[Au(PPh_3)(CNR)]^+ + [Pt(PPh_3)(CNR)] \longrightarrow [(CNR)_2(PPh_3)PtAu(PPh_3)]^+ \quad (6)$$

Scheme.

The cluster (**4**) could result from the sequence of ligand-exchange and oxidative-addition reaction shown in the Scheme (R = $C_6H_3Me_2$-2,6). According to the reactions shown in the Scheme $[Au(CNR)_2]^+$ acts initially as a phosphine acceptor generating a co-ordinatively unsaturated $[Pt(PPh_3)(CNR)]$ fragment which undergoes an oxidative-addition reaction with $[Au(PPh_3)(CNR)]^+$. Dimerisation of (**6**) by either an oxidative-addition reaction at gold or by a cycloaddition process leads to

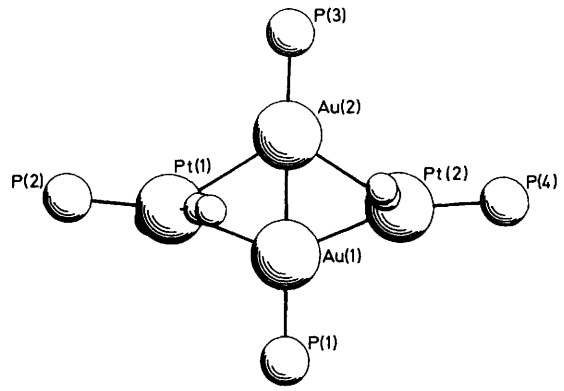

Figure 2. Illustration of the inner co-ordination sphere of $[Pt_2Au_2(PPh_3)_4(CNC_6H_3Me_2\text{-}2,6)_4]^{2+}$ viewed perpendicular to the best plane defined by the metal atoms

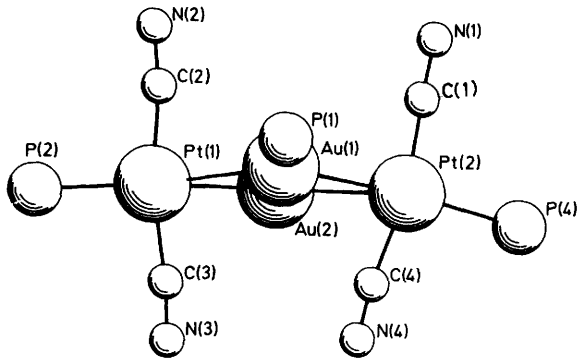

Figure 3. Illustration of the inner co-ordination sphere of $[Pt_2Au_2(PPh_3)_4(CNC_6H_3Me_2\text{-}2,6)_4]^{2+}$ showing the $Pt(PPh_3)(CNC_6H_3Me_2\text{-}2,6)_2$ fragments bridging the Au–Au bond

the alternative structures (**I'**) and (**II**) for (**4**). Structure (**I'**) represents an extension of the type of distortion observed for (**4b**) in the solid state and illustrated in (**I**). Chemically (**4**) was found to be remarkably stable to attack by nucleophiles, *e.g.* CO, PPh_3, and $CNC_6H_3Me_2$-2,6 and was not reduced by H_2 or Zn dust. The cluster was degraded by Na/Hg and $NaBH_4$, but the products were not easily isolated and have not been identified. The proposed structure of (**4**) is different from the tetrahedral skeletal geometry reported for other tetranuclear platinum–gold clusters.[6,7]

The relevant details of the *X*-ray crystallographic structural analysis for (**4b**) are given in the Experimental section. The fractional atomic co-ordinates are given in Table 2 and the structure of the cation is illustrated in Figures 2 and 3. Table 3 gives important bond lengths and angles. The structure can be described in terms of a flattened 'butterfly' skeletal geometry with a dihedral angle between Pt(1)–Au(1)–Au(2) and Pt(2)–Au(1)–Au(2) of 168.89(6)°. The platinum atoms are located at the wing-tip positions of the butterfly. Two isocyanides and one phosphine are co-ordinated to each platinum and define a distorted T-shaped environment [P(2)–Pt(1)–C(2) 95.2(9), P(2)–Pt(1)–C(3) 97(1), and C(2)–Pt(1)–C(3) 167(1)°]. The gold atoms are co-ordinated only to PPh_3 ligands, the $Au_2(PPh_3)_2$ groups being virtually linear [P(1)–Au(1)–Au(2) 175.7(2) and Au(1)–Au(2)–P(2) 170.9(2)°].

The butterfly structure is not symmetrical and is distorted in a manner which reduces the idealised symmetry of the skeletal atoms from D_{2h} to C_{2v}. The Pt(1)–Au(1)–Pt(2) angle is *ca.* 135°

Table 4. Selected intramolecular bond lengths (Å) for platinum–gold clusters

Complex	Pt–Au	Au–Au
(3) $[Pt_3Au(SO_2)_2Cl\{P(C_6H_4F\text{-}p)_3\}\{P(C_6H_{11})_3\}_3]$[a]	2.766(1)—2.771(1)	—
(2) $[Pt_3Au(CO)_3\{P(C_6H_{11})_3\}_4]^+$[b]	2.750(5)—2.768(5)	—
$[Pt_3Au(SO_2)(CO)_2\{P(C_6H_{11})_3\}_4]$[a]	2.755(1)—2.759(5)	—
(1) $[PtAu_2Cl(PEt_3)_2(PPh_3)_2]^+$[c]	2.601(4) av.	2.737(3)

[a] Ref. 7. [b] Ref. 6. [c] Ref. 5.

and the phosphorus–platinum vectors are tilted towards Au(1) rather than the midpoint of the Au(1)–Au(2) bond. This leads to the following differences in bond angles: P(2)–Pt(1)–Au(1) 162.9(2), P(4)–Pt(2)–Au(1) 160.9(2), Pt(1)–Au(1)–Pt(2) 134.97(6), and Pt(1)–Au(2)–Pt(2) 114.90(5)°. The asymmetry is also reflected in the Au(1)–Pt distances, which are at least 0.2 Å shorter than Au(2)–Pt [*i.e.*, Au(1)–Pt(1) 2.718(2), Au(1)–Pt(2) 2.712(2), Au(2)–Pt(1) 3.028(2), and Au(2)–Pt(2) 2.922(2) Å]. The former are comparable to the sum of the metallic radii (2.8 Å) whereas the latter are at the limits of significant metal–metal bonding. Table 4 gives gold–gold and platinum–gold bond lengths for the other known platinum–gold clusters. The Au(1)–Pt bonds are comparable in length with those found in the tetrahedral clusters but are longer than the Pt–Au bonds in (**1**). The Au–Au bond length of 2.593(2) Å in (**4b**) is one of the shortest reported and is significantly shorter than that found in (**1**). Linearity of an $Au_2(PR_3)_2$ unit would be predicted to lead to a short Au–Au bond due to a large overlap of the two out-pointing *sp* hybrids on each gold atom. On distorting the geometry from linearity about the gold a lengthening of the bond would be expected (see below). This change is reflected in

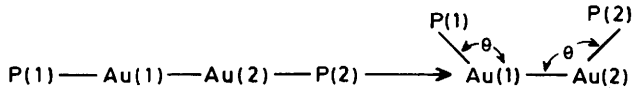

the computed reduced overlap populations for $Au_2(PH_3)_2$. For linear $Au_2(PH_3)_2$ ($\theta = 180°$), the computed reduced overlap population is 0.658 and for $\theta = 90°$ the computed reduced overlap population is 0.342. In order to confirm this hypothesis the Cambridge Crystallographic Data Base was searched for all structures containing the Au_2P_2 unit. Any Au_2P_2 unit which showed a torsion angle [P(1)–Au(1)–Au(2)–P(2)] greater than 10° and showed P(1)–Au(1)–Au(2) differing from Au(1)–Au(2)–P(2) by more than 10° were rejected in the subsequent analysis. Figure 4 shows a scatterplot of θ(°) *versus* Au–Au bond length (Å). Short Au–Au bond lengths are found if the Au_2P_2 unit is linear, however there is a poor correlation between θ and bond length. This arises because the statistical analysis is dominated by the high frequency of data when θ lies between 110 and 140° and the low frequency of data for linear Au_2P_2 fragments. This analysis suggests that the Au–Au bond lengths in such molecules are not only determined by the Au–Au–P bond angles but that other steric and electronic effects are in operation.

In a subsequent paper[9] a detailed analysis of the bonding in platinum–gold cluster compounds will be presented and therefore only a brief summary of the bonding interactions in $[Pt_2Au_2(PPh_3)_4(CNC_6H_3Me_2\text{-}2,6)_4]^{2+}$ will be given below. The $[Pt(PPh_3)(CNC_6H_3Me_2\text{-}2,6)_2]^+$ and $Au(PPh_3)$ fragments are isolobal[10,11] and their bonding capabilities are dominated by an out-pointing orbital of a_1 symmetry[11] [see (**III**) and (**IV**)]. Furthermore, a single electron resides in the out-pointing

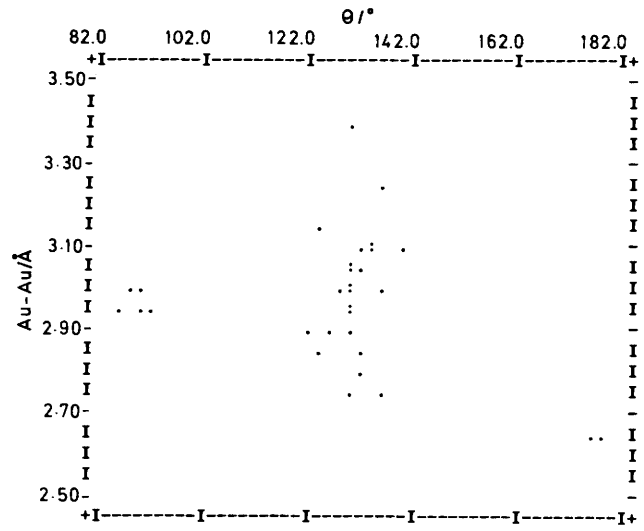

Figure 4. Scatterplot of θ (°) *versus* Au–Au bond length (Å); 36 points plotted, correlation coefficient = −0.290

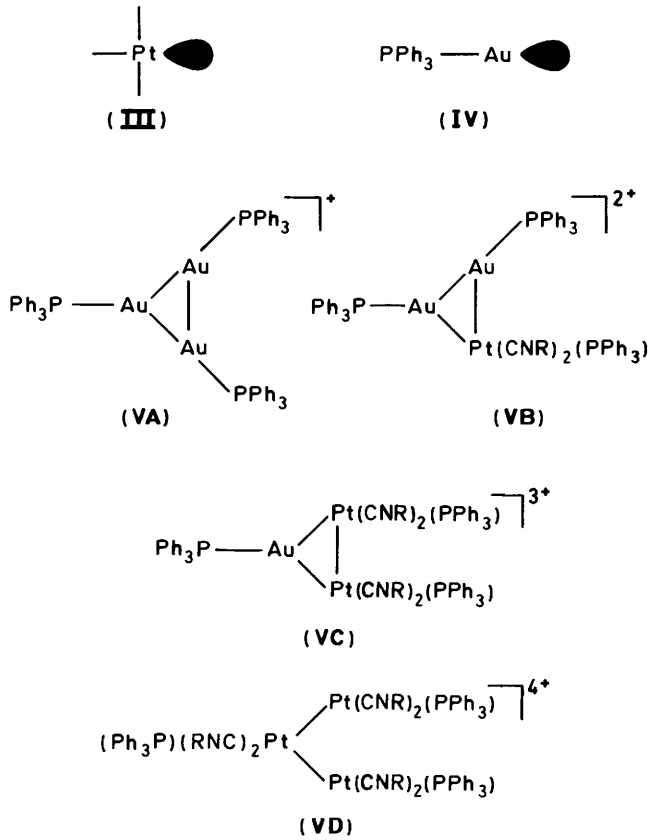

orbitals of each fragment. In triangular clusters based on these fragments the bonding between the metal atoms can be described in terms of a three-centre two-electron bond leading to the series of related molecules (**VA**)—(**VD**) (R = $C_6H_3Me_2$-2,6).

Braunstein's compound $[PtAu_2Cl(PEt_3)_2(PPh_3)_2]^+$ (**1**)[5] is isoelectronic with (**VB**). In $[Pt_2Au_2(PPh_3)_4(CNC_6H_3Me_2\text{-}2,6)_4]^{2+}$ (**4**), with an idealised D_{2h} skeletal geometry, the bonding can also be described in terms of a pair of three-centre two-electron bonds leading to a total valence electron count of 56 electrons. However, this can only be achieved if the gold

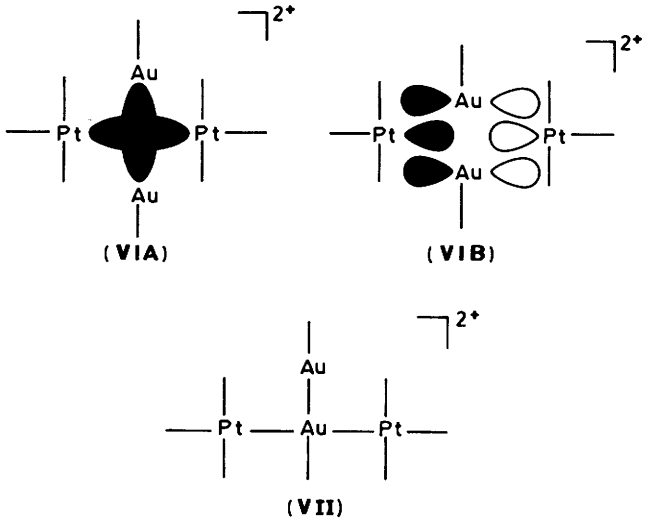

6*p* orbitals perpendicular to the Au–P bonds also make a substantial bonding contribution. The molecular orbital representations which describe the bonding are illustrated by (**VIA**) and (**VIB**). Since the gold 6*p* orbitals are rather high lying their contribution to (**VIB**) is smaller than the contribution of the gold 6*s* orbitals to (**VIA**). Indeed, detailed calculations have demonstrated that the loss of overlap between the platinum fragments and those of the gold atoms when the structure is distorted in the manner illustrated in (**VII**) is small, leading to a soft potential-energy surface for this distortion co-ordinate. The bonding in (**VII**) can be described in terms of localised two-centre two-electron bonds. It is a mixed valence structure based on Au^{I} and Au^{III} centres. The structure observed for $[Pt_2Au_2(PPh_3)_4(CNC_6H_3Me_2\text{-}2,6)_4]^{2+}$ in the solid state lies on a reaction co-ordinate connecting (**VI**) and (**VII**).

Experimental

Reactions were routinely carried out using standard Schlenk-line procedures under an atmosphere of pure dry N_2 and using dry dioxygen-free solvents. Microanalyses (C, H, and N) were carried out by Mr. M. Gascoyne and his staff at this Laboratory. Grating i.r. spectra were recorded as Nujol mulls using a Pye-Unicam SP2000 spectrometer. Fourier-transform i.r. spectra were recorded as Nujol mulls using a Perkin-Elmer 1710 spectrometer. Electronic spectra were recorded on a Perkin-Elmer 552 u.v.–vis. spectrophotometer, using 10-mm quartz cells. Melting points were recorded on an Electrothermal melting point apparatus. The *X*-ray microanalysis was performed by Mrs. A. Stoker of the Chemical Crystallography Laboratory, Oxford on a JEOL 2000FX analytical electron microscope.

Proton-decoupled $^{31}P\text{-}\{^1H\}$ and $^{195}Pt\text{-}\{^1H\}$ n.m.r. spectra were recorded using a Bruker A.M.250 spectrometer. Samples for $^{31}P\text{-}\{^1H\}$ were referenced relative to $PO(PMe)_3$ and $^{195}Pt\text{-}\{^1H\}$ to $Na_2[PtCl_6]$ in D_2O. The machine operating frequencies were 161.26 MHz for ^{31}P and 53.55 MHz for ^{195}Pt. N.m.r. computer simulations were carried out using the Oxford University VAX computer systems using a program developed by Professor R. K. Harris at the University of East Anglia and adapted for use at Oxford by Dr. A. E. Derome. Complexes $[Pt(PPh_3)_2(C_2H_4)]$ and $[Au(CNC_6H_3Me_2\text{-}2,6)Cl]$ were synthesised by literature methods;[12,13] $[Pt(PPh_3)_2(C_2H_4)]$ was recrystallised under ethylene (1 atm, 10^5 Pa) from CH_2Cl_2–hexane.

Synthesis of $[Au(CNC_6H_3Me_2\text{-}2,6)_2]PF_6$.—$[Au(CNC_6H_3Me_2\text{-}2,6)Cl]$ (0.21 g, 0.58 mmol) was suspended in a 1:1 mixture of CH_2Cl_2–EtOH (40 cm^3) and $CNC_6H_3Me_2$-2,6 (0.076 g, 0.58 mmol) was added with stirring. The suspension was refluxed gently at 50 °C until the suspension dissolved and the solution then allowed to cool with stirring. The solution was concentrated to low volume and NH_4PF_6 (0.5 g) was added to yield a white precipitate. The precipitate was washed with benzene, ethanol, and diethyl ether and recrystallised from CH_2Cl_2–hexane. Yield: 90% (Found: C, 35.8; H, 2.2; N, 4.3. $C_{18}H_{18}AuF_6N_2P$ requires C, 35.8; H, 3.0; N, 4.6%); ν(CN) (Nujol) at 2 231 cm^{-1}, $\nu(PF_6^-)$ at 840 cm^{-1}. The BF_4^- salt was prepared in an analogous manner by the addition of $NaBF_4$ (0.5 g) after the refluxing stage (Found: C, 37.6; H, 3.2; N, 5.0. $C_{18}H_{18}AuBF_4N_2$ requires C, 38.2; H, 3.2; N, 4.9%).

Synthesis of $[Pt_2Au_2(PPh_3)_4(CNC_6H_3Me_2\text{-}2,6)_4][PF_6]_2$ (**4b**).—$[Au(CNC_6H_3Me_2\text{-}2,6)_2]PF_6$ (0.21 g, 0.35 mmol) was added to $[Pt(PPh_3)_2(C_2H_4)]$ (0.26 g, 0.35 mmol) in acetone (40 cm^3) with stirring. The solution immediately deepened to a blood red colour. After stirring for 1 h the solution was concentrated to low volume (20 cm^3) and diethyl ether was slowly added to yield dark brown crystals. The supernatant liquid was filtered off and the crystals washed with benzene and diethyl ether and dried *in vacuo*. Yield: 0.27 g, 60% (Found: C, 49.1; H, 3.8; N, 2.1. $C_{108}H_{96}Au_2F_{12}N_4P_6Pt_2$ requires C, 49.0; H, 3.7; N, 2.1%); ν(CN) (Nujol) at 2 130 cm^{-1}, $\nu(PF_6^-)$ at 840 cm^{-1}; m.p. 164—167 °C. U.v. (CH_2Cl_2): $\lambda_{max.}$ 345, 375, 425(sh) nm. A suitable crystal for crystallography was grown from acetone–diethyl ether.

The BF_4^- salt (**4a**) was prepared in an analogous manner by addition of 1 mol equivalent of $[Au(CNC_6H_3Me_2\text{-}2,6)_2]BF_4$ to $[Pt(PPh_3)_2(C_2H_4)]$ (Found: C, 51.7; H, 3.9; N, 2.3. $C_{108}H_{96}Au_2BF_4N_4P_4Pt_2$ requires C, 51.5; H, 3.8; N, 2.2%); m.p. 176—180 °C (decomp.); ν(CN) (Nujol) at 2 130 cm^{-1}, $\nu(BF_4^-)$ at 1 100 cm^{-1}.

Analytical and Crystal Data for $[Pt_3(PPh_3)_2(CNC_6H_3Me_2\text{-}2,6)_6][PF_6]_2$ (**5b**).—A single crystal was grown by slow diffusion of diethyl ether into an acetone solution of (**5b**) (Found: C, 48.5; H, 4.0; N, 3.5. $C_{90}H_{84}F_{12}N_6P_4Pt_3$ requires C, 49.4; H, 3.8; N, 3.8%). The crystal was mounted on an Enraf–Nonius CAD4(F) automatic four-circle diffractometer using Mo-K_α (λ = 0.710 69 Å) radiation with a graphite monochromator. After manually centring the crystal the unit-cell parameters were found from the setting angles of 25 strong reflections: a = 11.85(6), b = 13.911(2), c = 14.78(1) Å, α = 82.6(1), β = 67.87(6), γ = 89.5(1)°, and U = 2 237 $Å^3$. A more detailed discussion of the structural analysis will appear in a future publication.[8]

Single-crystal X-*Ray Structural Determination of* $[Pt_2Au_2(PPh_3)_4(CNC_6H_3Me_2\text{-}2,6)_4][PF_6]_2$ (**4b**).—*Crystal data*. $C_{108}H_{96}Au_2F_{12}N_4P_6Pt_2$, M = 2 647.7, triclinic, space group $P\bar{1}$, a = 13.882(4), b = 15.460(2), c = 27.578(5) Å, α = 77.99(5), β = 88.95(2), γ = 67.41(5)°, U = 5 326 $Å^3$, D_c = 1.65 g cm^{-3}, Z = 2, $F(000)$ = 2 568.0, μ(Mo-K_α) = 57.45 cm^{-1}.

Data collection and reduction. A suitable crystal for the *X*-ray work was sealed in a 0.5-mm Lindemann tube. The crystal was then mounted on an Enraf–Nonius CAD4(F) automatic four-circle diffractometer using Mo-K_α (λ = 0.710 69 Å) radiation with a graphite monochromator. After manually centring the crystal an automatic reflection search routine located 25 reflections which were used to determine an orientation matrix and unit-cell parameters. Intensity data were collected at *ca.* 297 K using an ω–2θ scan technique with scan width = 0.90 + 0.35 tanθ. Horizontal aperture parameters A, B (mm) in APT = A + B tanθ were 3.00,0.0. Standard

reflections were remeasured at regular intervals. These reflections dropped systematically to 50% of their original value during data collection indicating significant decomposition. For the purpose of computing an absorption correction, ψ-scan profiles were obtained for two reflections. These showed a variation of *ca.* 30%. The data were corrected for Lorentz, polarisation, and absorption effects; equivalent reflections were merged and systematically absent reflections were removed. A total of 5 747 reflections were measured, of which 3 930 having $I \geqslant 3\sigma(I)$ were used for the structure solution and refinement.

Structure solution and refinement. The metal atoms were located by heavy-atom methods using a Patterson map. The remaining non-hydrogen atoms were located from successive difference electron-density maps. The positions of the phenyl and isocyanide hydrogen atoms were calculated assuming a C–H bond length of 0.98 Å and assuming idealised geometries.

All non-hydrogen atoms were refined using blocked-matrix least squares and the positional and thermal parameters were refined in separate blocks. The platinum, gold, and phosphorus atoms were refined anisotropically and the carbon atoms isotropically. Throughout the refinement the phenyl groups were restrained to their idealised geometries within specified limits.

During the final stages of refinement (588 parameters) a Chebyshev weighting scheme (coefficients 28.22, 34.57, 11.57) was employed. Each reflection was assigned a weight $w = 1/r\sum_{r=1}^{n} A_r T_r(X)$ where n is the number of coefficients, A_r, for a Chebyshev series, T_r is the polynomial function and X is $F_o/F_o(\text{max.})$.

The refinement converged with $R\ (=\Sigma\Delta F/\Delta F_o) = 0.054$ and $R'\ [=(\Sigma w\Delta F^2/\Sigma wF_o^2)^{\frac{1}{2}}] = 0.071$. Neutral scattering factors were taken from ref. 14 and anomalous scattering factors were taken from ref. 15. All crystallographic calculations and diagrams were made using CRYSTALS and CHEMGRAF systems [14] on a DEC VAX 11/750 computer in the Department of Chemical Crystallography, Oxford.

Acknowledgements

We thank the S.E.R.C. for financial support, Johnson-Matthey for generous loans of gold and platinum metals, and Mr. D. Sherman for recording the n.m.r. spectra.

References

1 M. J. Freeman, M. Green, A. G. Orpen, I. D. Salter, and F. G. A. Stone, *J. Chem. Soc., Chem. Commun.*, 1983, 1332 and refs. therein.
2 K. P. Hall and D. M. P. Mingos, *Prog. Inorg. Chem.*, 1984, **32**, 237.
3 A. J. Layton, R. S. Nyholm, G. A. Pneumaticakis, and M. L. Tobe, *Chem. Ind.*, 1967, 465.
4 C. E. Briant, D. I. Gilmour, and D. M. P. Mingos, *J. Organomet. Chem.*, 1984, **267**, C52.
5 P. Braunstein, H. Lenner, D. Matt, A. Tiripicchio, and M. Tiripicchio-Camellini, *Angew. Chem., Int. Ed. Engl.*, 1984, **96**, 307.
6 C. E. Briant, R. W. M. Wardle, and D. M. P. Mingos, *J. Organomet. Chem.*, 1984, **267**, C49.
7 D. M. P. Mingos and R. W. M. Wardle, *J. Chem. Soc., Dalton Trans.*, 1986, 73.
8 C. E. Briant, D. I. Gilmour, and D. M. P. Mingos, *J. Organomet. Chem.*, submitted for publication.
9 D. I. Gilmour and D. M. P. Mingos, *J. Organomet. Chem.*, in the press.
10 D. L. Thorn and R. Hoffmann, *J. Am. Chem. Soc.*, 1978, **100**, 2079.
11 D. G. Evans and D. M. P. Mingos, *J. Organomet. Chem.*, 1982, **232**, 171.
12 U. Nagel, *Chem. Ber.*, 1982, **115**, 1998.
13 F. Bonati and G. Minghetti, *Gazz. Chim. Ital.*, 1973, **103**, 373.
14 J. R. Carruthers, CRYSTALS User Manual, Oxford University Computing Centre, 1975; K. Davies, CHEMGRAF User Manual, Chemical Crystallography Laboratory Oxford, 1981; 'International Tables for *X*-Ray Crystallography,' Kynoch Press, Birmingham, vol. 4.
15 D. T. Cromer and J. B. Mann, *Acta Crystallogr., Sect. A*, 1968, **24**, 1968.

Received 19*th June* 1985; *Paper* 5/1033